A <5 dB NF, >17 dBm $OP_{1 \text{ dB}}$ F-Band GaN-on-SiC HEMT LNA with a Monolithic Substrate-Integrated Waveguide Filter

Fabian Thome[#], Dirk Schwantuschke[#], Peter Brückner[#], Xiaopeng Wang^{\$}, James C. M. Hwang^{\$}, Rüdiger Quay[#]

*Fraunhofer Institute for Applied Solid State Physics IAF, Germany *Cornell University, USA

Fabian.Thome@iaf.fraunhofer.de

Abstract — This paper demonstrates the monolithic integration of a substrate-integrated waveguide bandpass filter (BPF) and a low-noise amplifier (LNA) at F-band, fabricated in a 70-nm GaN-on-SiC technology. The three-stage LNA alone achieves a state-of-the-art average noise figure of 3.6 dB over 87–115 GHz. The LNA + BPF exhibits a peak gain of 13.6 dB over a 3 dB bandwidth of 17 GHz from 104 to 121 GHz. The average noise figure is 4.9 dB over 87–115 GHz. The $OP_{1 \text{ dB}}$ and saturated output power are 17.6 dBm and >20 dBm, respectively.

Keywords — Bandpass filter (BPF), gallium nitride (GaN), high-electron-mobility transistors (HEMTs), low-noise amplifiers (LNAs), millimeter wave (mmW), monolithic microwave integrated circuits (MMICs), substrate-integrated waveguide (SIW).

I. Introduction

In many applications, receiver (Rx) front-ends face severe linearity and robustness constrains, either to handle high in-band input signals or to maintain linear operation with strong signals. In wireless communications, the high signal level of an adjacent channel or a strong interfering signal can lead to compression and intermodulation issues. Furthermore, an extremely strong in-band input signal can damage the active devices of the LNA. Thus, many wireless communication or radar systems require a bandpass filter (BPF) and an RF limiter in front of the LNA to improve the linearity of the Rx and to protect the LNA from being destroyed, respectively. However, at millimeter-wave frequencies, either the high insertion loss of planar filters, leading to a severe noise-figure (NF) degradation, or the high cost and form factor of classical waveguide filters are a major challenge. Substrate-integrated waveguide (SIW) BPFs can have the benefit of a monolithic integration together with the LNA omitting assembly losses between LNA and BPF, while having low losses and high power-handling capacities comparable to a classical air-filled waveguide filter. Moreover, in comparison to other transistor technologies, GaN HEMT technologies offer the possibility to omit the limiter leading to similar advantages of a reduced system NF as for the BPF. Thus, the system noise performance can benefit twice when monolithically integrating an SIW BPF in front of a GaN HEMT LNA.

In literature, the best noise performance is demonstrated by InGaAs-on-GaAs HEMT technologies with an NF of below 2 dB at 110 GHz [1]. However, the linearity is limited with the output power at 1-dB compression $(OP_{1\,dB})$ approx. 0 dBm.

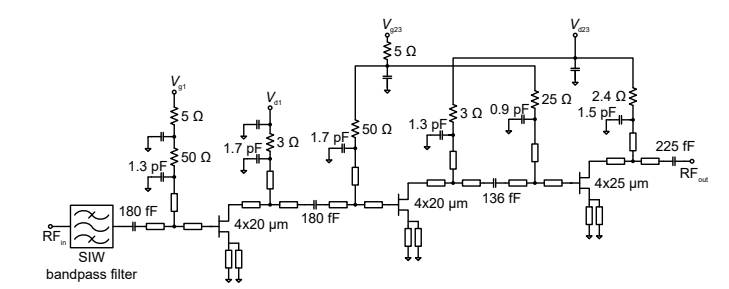


Fig. 1. Simplified schematic of the MMIC containing a three-stage LNA and an integrated SIW BPF.

On a silicon substrate with an InGaAs channel, the lowest *NF* at 100 GHz is 3.5 dB [2]. For Si MOSFET and SiGe HBT technologies, the best *NF* is more than 4 dB [3]–[5], *OP*_{1 dB} is below 0 dBm. Furthermore, the above-mentioned technologies tend to be sensitive to extremely large input signal making a limiter in front of the LNA in many applications necessary. A more detailed comparison of LNA MMICs around 110 GHz is shown in Table 1. At this frequency range, no LNA with a monolithic-integrated input BPF was found in literature. Air-filled waveguide filters provide an excellent stop-band rejection of up to 90 dB, however, the insertion loss at 100 GHz is in the range of 1–1.5 dB [6].

This work presents a monolithic integration of a three-pole SIW BPF with a three-stage LNA fabricated in a GaN-on-SiC HEMT technology. The monolithic microwave integrated circuit (MMIC) targets a 105–120-GHz band with a high suppression of interfering signals.

II. LNA MMIC DESIGN

A simplified schematic of the LNA MMIC is illustrated in Fig. 1 together with the integrated BPF. The LNA consists of three common-source (CS) stages. The gate width in each stage is a major design decision, which, however, depends as well on the use of source lines. Inductive source degeneration (ISD) is commonly used in the first stage of LNAs for an improved simultaneous input noise and power matching. Therefore, Fig. 2 shows a contour plot of the simulated maximum gain (MSG/MAG) and minimum NF (NF_{min}) for different unit gate widths (UGW) and source line lengths (SLL). As it can be seen, MSG increases with increasing the SLL. This is due to a compensation of the gate-drain capacitance by the introduced source inductance [10]. To increase the overall gain, ISD is

Table 1. State-of-the-Art LNA MMICs With an Operating Frequency in the Range of 110 GHz

Reference	Technology	f _T /f _{max} (GHz)	Topology	3-dB BW (GHz)	S ₂₁ (dB)	P_{dc} (W)	$OP_{1dB}\ (dBm)$	P _{sat} (dBm)	NF (dB)
[1]	50-nm InGaAs mHEMT	380/670	4-stage CS	35* (75–110)	>24	25.5	>0	n/a	av 1.7 (1.5–2) (75–110 GHz)
[2]	20-nm InGaAs-on-Si	200/640	4-stage CS	68* (59–127)	>15	33.3	n/a	n/a	av 3.5 (3.1–4.1) (75–105 GHz)
[7]	35-nm InGaAs mHEMT	>500/>1000	distributed	330*	>10	346	8	11.8	av 3.7 (75–150 GHz)
[8]	70-nm GaN HEMT	145/>300	5-stage CS	42* (80–122)	>24	1840	18.9–21.2	22.8-24.3	av 3.9 (3.5-5.5)
[9]	70-nm GaN HEMT	145/>300	5-stage CS	53* (102–155)	>16.2	533	5.4–13.7	9.5–17.5	av 4.7 (3.6–5.6) (110–150 GHz)
[3]	0.13-μm SiGe BiCMOS	350/450	3-stage CE	30 (75–105)	16.4	n/a	n/a	n/a	4–6 (75–105 GHz)
[4]	22-nm CMOS FDSOI	220/380	3-stage RF cascode	31 (77–108)	18.2	16	–5.5 @ 94 GHz	–2.5 @ 94 GHz	5.8-6.6 (94-96 GHz)
[5]	40-nm CMOS	265/280	8-stage CS	40.6* (101.5–142.1)	20.6	45	−3.1 @ 120 GHz	2	av 6.2 (110–130 GHz)
This work	70-nm GaN HEMT	145/>300	3-stage CS	45* (74–119)	>13	660	16–17.8 (80–110 GHz)	>20	av 3.6 (3.2–4) (87–115 GHz)
			3-stage CS + SIW BPF	17 (104–121)	13.6		17.6–17.8 (105–110 GHz)	>20	av 4.9 (4.4–5.8) (106–115 GHz)

^{*} No 3-dB BW.

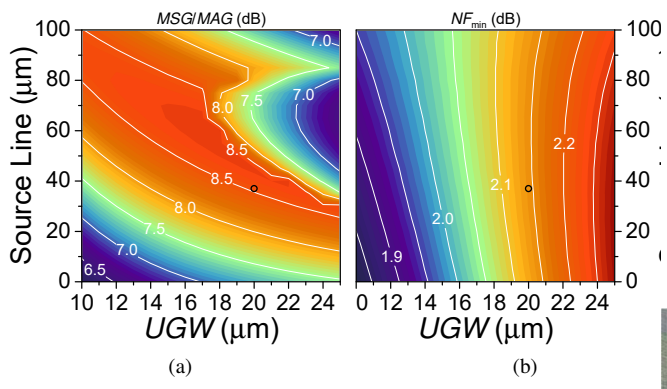
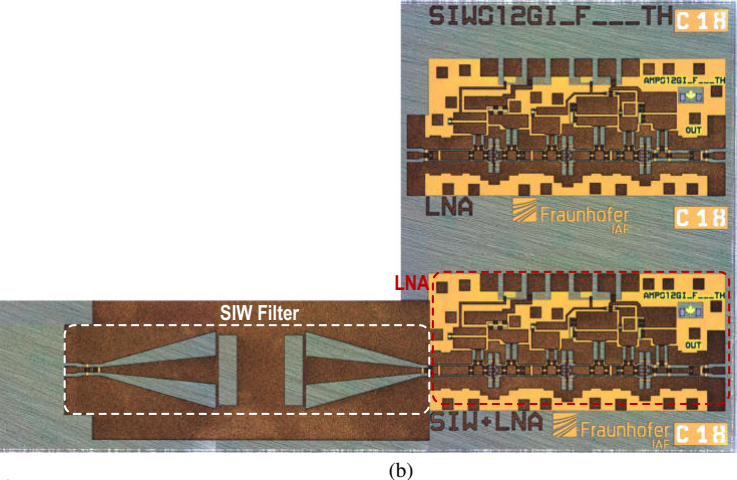


Fig. 2. Simulated contour of (a) MSG/MAG and (b) NF_{min} at 110 GHz.

used in all stages. The first two (most noise relevant) stages use transistors with a total gate width of $80~\mu m$ and an UGW of $20~\mu m$. This allows as well for a simple, low-loss matching of the input to $50~\Omega$. The SLL is $37~\mu m$, which improves the MSG by more than 1 dB compared to a CS device with the same gate width. The sudden gain drop for UGW above $18~\mu m$ and SSL between $40-80~\mu m$ shows the MAG region and should be avoided in this context due to the reduced gain. In the output stage, the total gate width is increased to $100~\mu m$ for improving the output power and linearity. The dc gate and drain lines of the second and third stage are connected together in order to simplify the biasing of the MMIC, while maintaining the ability to adjust the bias of the input stage alone.

The BPF in front of the LNA consists of two parts. Tapered sections at the input and output of the filter to transition from a grounded coplanar waveguide at the RF input pad to an SIW resonator and then from the SIW resonator to the LNA input matching network. The SIW resonator has two rectangular gaps in the topside ground plane. The entire structure forms a three-pole filter with a total length of $1426 \, \mu m$. The simulated



SIW012GI_F

Fig. 3. Photographs of the fabricated chips containing (a) the LNA (stand-alone) and (b) the monolithic integration of SIW filter and LNA. Die size – LNA: $1.35 \times 0.58 \text{ mm}^2$; BPF + LNA: $2.8 \times 0.7 \text{ mm}^2$.

insertion loss of the BPF in the pass band is 1 dB [11].

The monolithic integration of the LNA and BPF is implemented in a GaN HEMT technology fabricated on 75- μ m-thick semi-insulating SiC substrates with a diameter of 100 mm [12]. The technology features transistors with a gate length of 70, 100, and 130 nm. In this work, 70 nm devices with a maximum f_T of 145 GHz are used. The first test structure is the LNA without BPF to allow for a characterization of the LNA alone. The second test structure is an integration of BPF and LNA. A chip photograph of the fabricated LNA and LNA plus SIW BPF is shown in Fig. 3. The LNA is biased with a drain-source voltage of 7.5 V and a drain current in the first, second, and third stage of 16, 32, and 40 mA, respectively. This leads to a total power consumption of 660 mW.

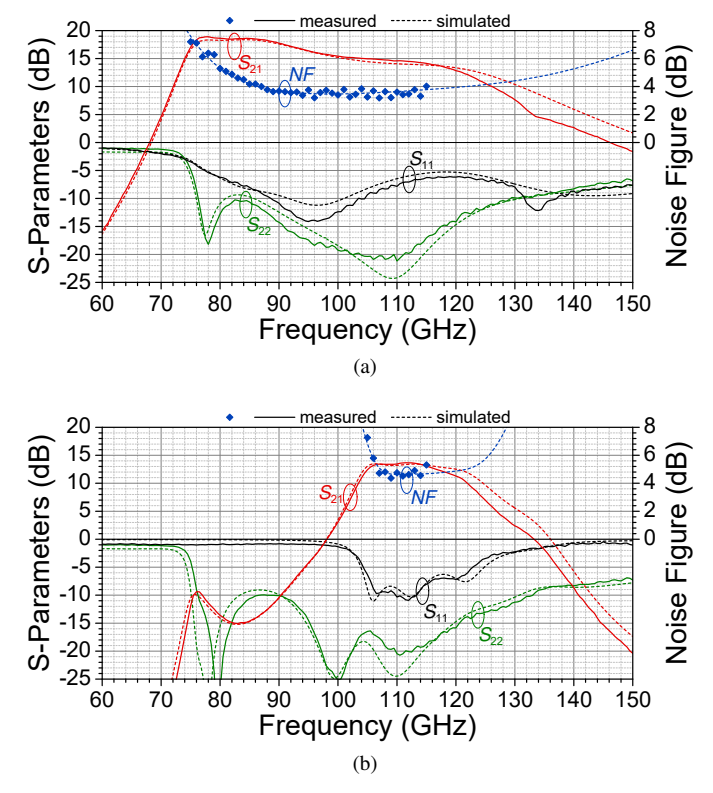


Fig. 4. Measured (solid lines and symbols) and simulated (dashed lines) S-parameters and NF of (a) the LNA and (b) the LNA with integrated filter.

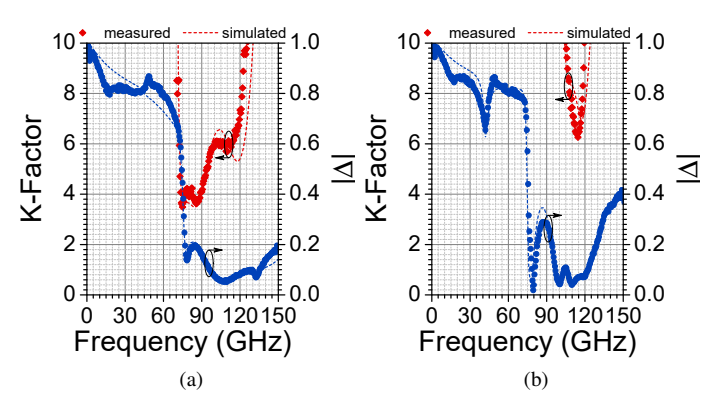


Fig. 5. Measured and simulated stability of (a) the LNA and (b) BPF + LNA.

III. MEASUREMENT RESULTS

The S-parameters are tested with the first setup consisting of an Anritsu VectorStar vector network analyzer from 10 MHz to 150 GHz. The probe tip calibration is done with an eLRRM algorithm and a Form Factor impedance standard substrate. The measured and simulated S-parameters of the LNA and BPF + LNA are shown in Fig. 4. The LNA (alone) achieves a maximum gain of 18.9 dB at 78 GHz. S_{21} is above 13 dB from 74–119 GHz. The integrated BPF + LNA has a peak gain of 13.6 dB across a 3-dB bandwidth of 17 GHz from 104 to 121 GHz. As intended, the lower band edge shows a steep slope suppressing unwanted out-of-band signals by more than 25 dB from 104 GHz down to 84 GHz.

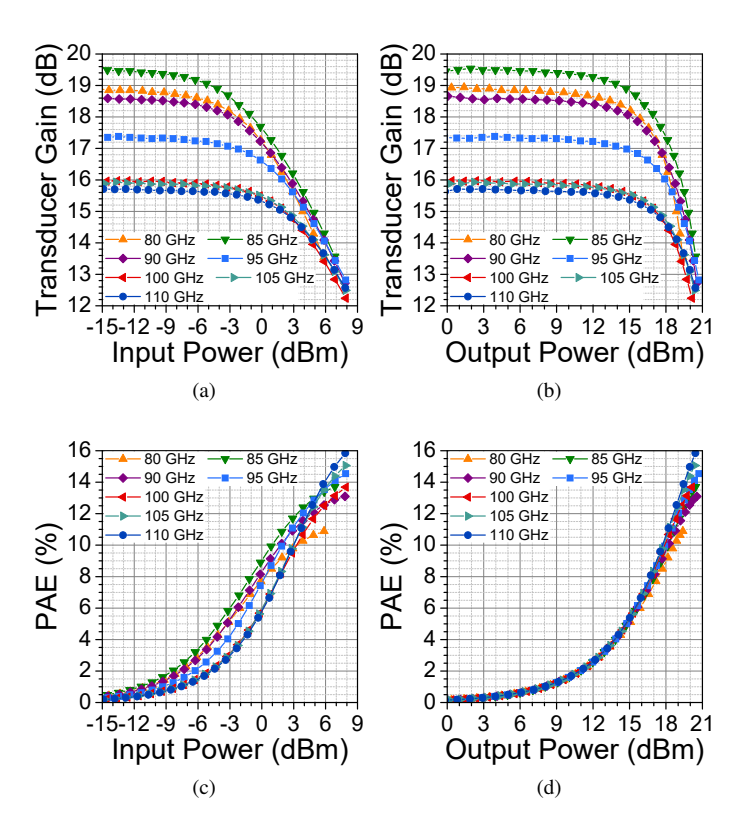


Fig. 6. Measured CW large-signal performance of the LNA.

Fig. 5 shows Rollett's stability factor of both test structures indicating unconditional stability over the entire measured frequency range from 10 MHz to 150 GHz.

The *NF* is measured with a second setup in a commonly-known Y-factor method with a WR10 waveguide noise source at the input and a subharmonic mixer module at the output, which converts the test signal down to 53 MHz. The actual noise power is measured by a Keysight *NF* analyzer. A Keysight signal generator is used as the LO signal source. The setup is calibrated to the RF probe tips. The measured *NF* of both test structures is shown together with the S-parameters in Fig. 4. The measured *NF* of the LNA (alone) is below 4 dB over 87–115 GHz with an average value of 3.6 dB. The BPF + LNA exhibits a measured minimum *NF* of 4.4 dB with an average value of 4.9 dB over 106–115 GHz. The difference of the measured *NF* between LNA with and without BPF reveals an insertion loss of the BPF of about 1.3 dB, which is close to the simulated value.

The large-signal measurements are done with a third setup containing a Keysight power meter plus a waveguide power sensor at the output. The input signal is provided by a Keysight signal generator with a connected HP multiplier-by-six module. The measured large-signal performance of the LNA alone is given in Fig. 6. For a constant input power of 8 dBm and frequencies above 80 GHz, the LNA yields a saturated output power of more than 20 dBm and a power-added efficiency (PAE) of 13–16%. The LNA exhibits an $OP_{1\,\mathrm{dB}}$ of better than 16 dBm over the entire measured band and peak

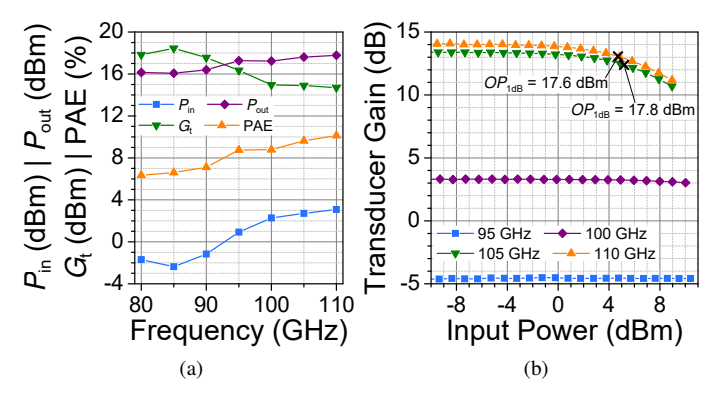


Fig. 7. (a) Measured performance at $P_{1\,\mathrm{dB}}$ of the LNA. (b) Measured large-signal performance of the LNA + BPF.

values of 17.6–17.8 dBm at 105–110 GHz [shown in Fig. 7(a)]. The PAE at $P_{1\,dB}$ is 10% at 110 GHz. Fig. 7(b) depicts a power sweep of the BPF + LNA at different frequencies. At 105 and 110 GHz, $OP_{1\,dB}$ is 17.6 and 17.8 dBm, respectively. This is similar to the stand-alone LNA and demonstrates that the SIW BPF does not affect $OP_{1\,dB}$ in the pass band as expected. It is important to mention that the BPF works as intended since out-of-band signals are suppressed, e.g., a 100-GHz signal by more than 10 dB, and indicating a compression of not even 0.3 dB up to an available input power of 10 dBm. At 95 GHz, the input signal is suppressed by 18 dB and the gain characteristic does not show any compression.

IV. DISCUSSION AND CONCLUSION

Table 1 summarizes the performance of the presented LNA and BPF + LNA, together with state-of-the-art LNA MMICs realized in different semiconductor technologies. The comparison reveals excellent noise performance with the highest $OP_{1\,dB}$ performance. With an average NF of 3.6 dB (87-115 GHz), this work demonstrates state-of-the-art GaN-HEMT LNA performance and an at least 0.4 dB lower NF compared to silicon-based technologies at 100 GHz or above [3]-[5]. Meanwhile, the measured $OP_{1 dB}$ is approximately 20 dB higher. Dedicated InGaAs HEMT low-noise technologies exhibit a record NF, which is almost 2 dB lower, however, $OP_{1 \text{ dB}}$ is more than 17 dB lower [1]. In this work, the LNA + BPF yields an average NF of 4.9 dB (106-115 GHz), which is still in the range of silicon-based technologies without an input filter. Meanwhile, the excellent large-signal performance of the stand-alone LNA is unaffected by the BPF. In addition, the SIW BPF can effectively prevent amplifier compression by large out-of-band signals. Furthermore, the robustness of GaN-HEMT technologies make it feasible to omit the commonly-needed limiter in front of the LNA. Thus, integrating an SIW BPF on a GaN-HEMT LNA MMIC demonstrates an important step for a further system NF improvement, while maintaining a robust Rx front-end architecture even without an input limiter.

ACKNOWLEDGMENT

The authors thank the colleagues in the epitaxy and technology departments of the Fraunhofer IAF for their excellent contributions during epitaxial growth and wafer processing.

REFERENCES

- [1] F. Thome et al., "Ultra-Low-Noise InGaAs mHEMT Technology and MMICs for Space Missions and Radio Astronomy," in IEEE MTT-S Int. Microw. Symp. Dig., Jun. 2023, pp. 1136–1139, doi: 10.1109/IMS37964.2023.10187960.
- [2] F. Thome, F. Heinz, and A. Leuther, "InGaAs MOSHEMT W-Band LNAs on Silicon and Gallium Arsenide Substrates," *IEEE Microw. Compon. Lett.*, vol. 30, no. 11, pp. 1089–1092, Nov. 2020, doi: 10.1109/LMWC.2020.3025674.
- [3] M. Varonen et al., "Cryogenic W-Band SiGe BiCMOS Low-Noise Amplifier," in *IEEE MTT-S Int. Microw. Symp. Dig.*, Jun. 2020, pp. 185–188, doi: 10.1109/IMS30576.2020.9223922.
- [4] L. Gao, E. Wagner, and G. M. Rebeiz, "Design of E- and W-Band Low-Noise Amplifiers in 22-nm CMOS FD-SOI," *IEEE Trans. Microw. Theory Techn.*, vol. 68, no. 1, pp. 132–143, Jan. 2020, doi: 10.1109/TMTT.2019.2944820.
- [5] T. H. Jang, K. P. Jung, J.-S. Kang, C. W. Byeon, and C. S. Park, "120-GHz 8-Stage Broadband Amplifier With Quantitative Stagger Tuning Technique," *IEEE Trans. Circuits Syst. I*, vol. 67, no. 3, pp. 785–796, Mar. 2020, doi: 10.1109/TCSI.2019.2958366.
- [6] Virginia Diodes. Waveguide Filter Operational Manual. [Online]. Available: https://www.vadiodes.com/images/Products/Passives/BPF/ ProductManual/VDI-738.1_Waveguide_Filter_Product_Manual.pdf
- [7] F. Thome and A. Leuther, "First Demonstration of Distributed Amplifier MMICs With More Than 300-GHz Bandwidth," *IEEE J. Solid-State Circuits*, vol. 56, no. 9, pp. 2647–2655, Sep. 2021, doi: 10.1109/JSSC.2021.3052952.
- [8] F. Thome, P. Brückner, S. Leone, and R. Quay, "A W/F-Band Low-Noise Power Amplifier GaN MMIC with 3.5–5.5-dB Noise Figure and 22.8–24.3-dBm P_{Out}," in *IEEE MTT-S Int. Microw. Symp. Dig.*, Jun. 2022, pp. 603–606, doi: 10.1109/IMS37962.2022.9865528.
- [9] F. Thome, P. Brückner, and R. Quay, "A D-Band Low-Noise Amplifier MMIC in a 70-nm GaN HEMT Technology," in Proc. Eur. Microw. Integr. Circuits Conf., Sep. 2023, pp. 5–8, doi: 10.23919/EuMIC58042.2023.10288876.
- [10] J.-A. Han, Z.-H. Kong, K. Ma, K. S. Yeo, and W. M. Lim, "Wideband millimetre-wave CMOS power amplifier using transistor-based inductive source degeneration and specially shielded transformer," *IET Microw. Antennas Propagat.*, vol. 11, no. 3, pp. 410–416, Dec. 2017, doi: 10.1049/iet-map.2016.0528.
- [11] X. Wang et al., "A Compact F-Band Filter Based on SiC Substrate-integrated Waveguides," in Proc. Asia–Pacific Microw. Conf., Dec. 2023, pp. 231–233, doi: 10.1109/APMC57107.2023.10439892.
- [12] F. Thome, P. Brückner, S. Leone, and R. Quay, "A Wideband E/W-Band Low-Noise Amplifier MMIC in a 70-nm Gate-Length GaN HEMT Technology," *IEEE Trans. Microw. Theory Techn.*, vol. 70, no. 2, pp. 1367–1376, Feb. 2022, doi: 10.1109/TMTT.2021.3134645.